Design of Non-Nucleoside Inhibitors of HIV-1 Reverse Transcriptase with Improved Drug Resistance Properties. 1.

Andrew L. Hopkins,[§,∞] Jingshan Ren,[§] John Milton,[Δ] Richard J. Hazen,[○] Joseph H. Chan,[○] David I. Stuart,[§,‡] and David K. Stammers*[,§,‡]

Division of Structural Biology, The Wellcome Trust Centre for Human Genetics, University of Oxford, Roosevelt Drive, Oxford, OX3 7BN, UK, Oxford Centre for Molecular Sciences, New Chemistry Building, University of Oxford, South Parks Road, Oxford, OX1 3QT, UK, GlaxoSmithKline Research and Development, Stevenage, Hertfordshire, U.K. and GlaxoSmithKline Research and Development, 5 Moore Drive, Research Triangle Park, North Carolina 27709

Received March 25, 2004

We have used a structure-based approach to design a novel series of non-nucleoside inhibitors of HIV-1 RT (NNRTIs). Detailed analysis of a wide range of crystal structures of HIV-1 RT−NNRTI complexes together with data on drug resistance mutations has identified factors important for tight binding of inhibitors and resilience to mutations. Using this approach we have designed and synthesized a novel series of quinolone NNRTIs. Crystal structure analysis of four of these compounds in complexes with HIV-1 RT confirms the predicted binding modes. Members of this quinolone series retain high activity against the important resistance mutations in RT at Tyr181Cys and Leu100Ile.

Introduction

Despite the advances in the available regimen of drugs to treat HIV-1 infection, there remains vital need to improve patient compliance, cost-of-goods and resistance profiles of each of the classes of anti-retroviral drugs. One of the four main classes of licensed anti-retroviral drugs are the non-nucleoside reverse transcriptase inhibitors (NNRTIs), the other three classes being nucleoside reverse transcriptase inhibitors, protease inhibitors and cell fusion inhibitors. The discovery of the first NNRTIs, HEPT[1,2] and TIBO,[3,4] opened a fruitful stream of research which eventually lead to three licensed drugs: nevirapine, delavirdine and efavirenz.[5]

The NNRTIs selectively inhibit HIV-1 reverse transcriptase by binding an allosteric site in a noncompetitive manner with respect to the substrate[6] and displacing the polymerase active site catalytic residues.[7] Unusually, the allosteric site appears to be formed only on binding of the NNRTIs to the viral enzyme. The particular 'plasticity'[6,8,9] of the NNRTI binding site has enabled the discovery of many structurally diverse classes of allosteric enzyme inhibitors, providing the medicinal chemist with a broad pallet from which to design improved anti-retrovirals.[10−12] However, NNRTIs have proven to be susceptibility to the rapid selection of drug resistance when evolutionary pressure is applied to the nonconserved binding site.

The dynamics of HIV replication and massive viral population constitute huge reservoirs of genetic variants in every single HIV infected patient.[13−15] Thus the challenge the medicinal chemist faces in designing improved NNRTIs is that every single-point NNRTI resistance mutations can be assumed to be present in the drug-naive HIV-1 population.[15,16] In this paper we attempt to synthesize the knowledge gained from crystallographic and mutational studies of HIV-1 reverse transcriptase into a set of medicinal chemistry strategies to improve the drug resistance profile of NNRTIs.

Spatial Distribution of Resistant Mutations. In the clinic the most commonly observed NNRTI resistance mutations are Tyr181Cys and Lys103Asn. However, the majority of residues lining the drug binding site have been observed to evolve drug resistance mutations when selection pressure is exerted on HIV-1 in vitro with a wider range of NNRTIs.[17−20]

Mapping the wealth of drug resistance sequence data onto the high-resolution protein crystal structures of the inhibited HIV-1 reverse transcriptase complex enables the medicinal chemist to observe trends that may be exploited in drug design. The observed drug resistance mutations selected by HIV-1 within the NNRTI pocket can be classified into three distinct categories (Figure 1). The mutations Val106Ala, Tyr181Cys, Tyr188Cys and Phe227Leu appear to confer resistance by reducing the contact surface area compared to the wild-type residues, thus presumably weakening the van der Waals interactions between the protein and the bound NNRTI.[21−23] There are some biochemical data supporting this interpretation at least for two of the residues. Studies of the pre-steady-state kinetics of the inhibition of Tyr181Cys RT by nevirapine indicate the mutation increases the K_d of inhibitor binding over 500-fold.[24] The decreased affinity of nevirapine is a consequence of the faster dissociation rate between the inhibitor and the Tyr181Cys RT enzyme, indicating a lower energy of interaction between the inhibitor and the mutant NNRTI pocket. Furthermore, steady-state kinetic experiments demonstrate the Val106Ala mutation increases the rate constant for nevirapine dissociation

* To whom correspondence should be addressed. E-mail: daves@strubi.ox.ac.uk.
§ Division of Structural Biology.
‡ Oxford Centre for Molecular Sciences.
Δ GSK Stevenage.
○ GSK RTP.
∞ Current address: Molecular Informatics, Structure and Design, Pfizer Global Research and Development, Sandwich, Kent, CT13 9NJ, U.K.

10.1021/jm040071z CCC: $27.50
Published on Web 10/23/2004

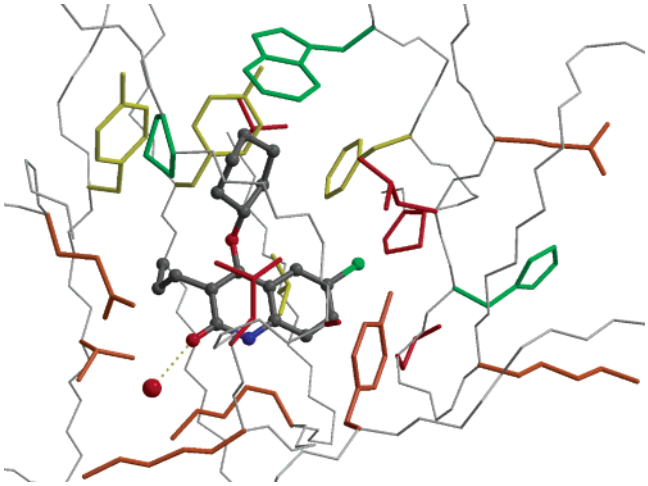

Figure 1. Physicochemical mechanisms of drug resistance. HIV-1 NNRTI resistance mutations are mapped onto the binding site of the mapped onto the NNRTI binding pocket from the crystal structure of the RT−**2a** complex. The inhibitor is shown as a ball-and-stick representation, and the surrounding residues are shown as thin sticks. The atoms are colored by type (grey − carbon; red − oxygen; blue − nitrogen; green − chlorine) and the water molecule as a red sphere. Mutations which confer resistance to NNRTIs by (a) loss of van der Waals contacts are colored yellow; (b) change of electrostatic charge or hydrogen bonding properties are colored orange; (c) steric hindrance with the inhibitor are colored red. Conserved residues, not been observed as drug resistant mutants are colored green. Partially conserved residues, which have only been observed as secondary or tertiary mutations against an existing drug resistant background are colored in a corresponding paler hue (residue 227 in pale yellow; residue 318 in pale orange; and residues 225 and 234 in pale red).

(k_{off}) by 8.5-fold,[25] supporting the assumption that this mutation confers resistance by reducing stabilizing interactions.

A second category of resistance mutations comprises Lys101Glu, Lys103Asn/Thr, Glu138Lys, Val179Asp, Glu233Val and Lys238Thr. These residues are positioned around the solvent channel in the NNRTI binding pocket, accessible to the bulk solvent. The mutations belonging to this second category either change the electrostatic charge or the hydrogen-bonding character compared to wild type. Steady-state kinetic experiments demonstrate the Lys103Asn mutation reduces the rate constant (k_{on}) for nevirapine binding[25] which together with structural studies[6,26] indicate that this particular mutation may influence the hydrogen bonding in the unliganded enzyme.

A third category of mutations can involve steric interference, either directly with the NNRTI or indirectly via the subtle repositioning of neighboring residues which appears to account for the action of the mutations Ala98Gly, Leu100Ile, Val108Ile, Gly190Ala/Glu, Pro225His, Pro236Leu and Leu234Ile. An example of this latter class would be the Val108Ile mutation, which is likely to act by altering the conformation of Tyr188. These residues, situated in the NNRTI pocket, undergo mutations that create steric clashes by subtle repositioning of the component atoms but generally do not have large changes in side chain bulk, possibly indicating that large residues would impair the function of the enzyme. Loss of enzyme function is exemplified by the Gly190Glu mutation, reported for quinoxaline derivatives HBY 097 and S-2720, which dramatically reduces viral replication competency by decreasing the enzymatic activity of RT to only 5% that of wild type.[27,28] The large increase in bulk on mutation from Gly to Glu at position 190 could occupy the NNRTI binding site and distort the polymerase catalytic site in an analogous way to the NNRTIs, in addition to the unfavorable positioning of a charged residue in the hydrophobic pocket. Such a mechanism would explain the preference for the virus to select for NNRTI mutations, which generally decrease the size of the residue side chain. The substitution of amino acid with larger residues may provide sufficient steric hindrance to provide substantial drug resistance but large amino acid substitutents may also, by analogy with the binding of an NNRTI, prove lethal by inducing conformational changes in the polymerase active site.

Structural Constraints on Drug Resistance. The number and variety of NNRTI resistance mutations may lead one to conclude the entire NNRTI pocket is mutable. Ultimately this is so, however, in terms of initial single and double drug resistance mutations there appear to be important structural constraints on protein stability and catalytic efficiency, which restrict the initial options for HIV-1 to mutate. The spatial relationship between the RT structure and the observed drug resistance mutations is visualized in Figure 1. The majority of the mutated residues cluster in a region near Tyr181 and in the solvent channel between Lys101 and Glu138(p51). Mapping of the mutational data demonstrates the presence of a 'conserved' region in the NNRTI pocket, comprising residues, which have not been reported to mutate as primary sources of resistance. The residues, which have not been primarily selected as drug resistance mutations are Pro225, Phe227, Trp229, Leu234 and Tyr318, all of which are highly conserved between other lentiviral RTs. The amino acids at positions 227 to 235 belong to the 'primer grip' region, responsible for maintaining the 3′-primer terminus in an orientation susceptible to nucleophilic attack by the incoming dNTP.[29−34]

The single point mutations Pro225His[35] and Phe227Leu[36] in recombinant RT increase resistance against several NNRTIs; however, mutations at positions 225 and 227 have only been observed to evolve as secondary mutations, appearing if the RT genetic background already contains the primary Val106Ala mutation.[37] Depending on the specific inhibitor, under dose-escalating passage experiments the selection of Val106Ala mutation may lead to the subsequent addition of either Pro225His (S-2720[38] or as a triple mutant against a Leu100Ile/Val106Ala background for HBY097[39]) or Phe227Leu (UC-781[37] and S-1153[36]). Site-directed mutation of Phe227 to Ala resulted in an RT which lacked 5′-RNA-directed RnaseH catalysis,[34] illustrating the cost of mutations in the 'primer grip' region. Sequential selection of Pro225His against the Val106Ala background has been proposed to arise due the additional stability of a potential hydrogen bond between the Nϵ2 atom of the mutated Pro225His to the main chain of residue 106.[38] Pro227His has also been observed as a double resistance mutation with Lys103Asn from patients on combination therapy that included efavirenz.[40] Interestingly Pro225His[35,38] and

Phe227Leu[36] sensitize RT to delavirdine (BHAP). Potentiation of delavirdine inhibition by the Pro225His mutation can be explained by the conformation of this residue, as observed in the RT−BHAP crystal structure.[35]

Trp229 is highly conserved among lentiviruses and has never arisen as a site for primary or secondary drug resistance mutation under selection pressure. The essential role of residue Trp229 has been investigated by mutagenesis, in which, the replacement of Trp229 with Ala exhibits a reduction in RNA and DNA-primed synthesis.[31,33,34,41,42] The Trp229Ala results in a mutant enzyme which shows a dramatic reduction in specific RNaseH cleavage function[33] and is incapable of forming a stable RT−template−primer replication complex.[32] Trp229 has been observed in two different conformations, where the ring system has been effectively flipped 180° by the Cβ-Cγ bond, the differing conformations can be observed even in structures of related inhibitor analogues.[8,43] Despite this structural flexibility, systematic site directed mutation of residue 229 reveals a steric preference for trytophan.[44] All other amino acids lead to a dramatic reduction in enzyme function to less than 1% of wild-type activity. Even aromatic substitutents, Phe and Tyr exhibit only 0.7% and 1.1% wild-type activity. Additionally recombinant virus strains with mutation at residue 229 were found to be unviable.[32,44]

A further 'conserved' residue in the region of the 'primer grip' part of the NNRTI pocket is Leu234. The importance of conserving Leu234 is demonstrated by the mutation of Leu234 to Asp resulting in noninfectious virus and a reduction in reverse transcriptase activity,[30] while the alteration of Leu234 to Ala produces a p66 subunit incapable of associating with the p51 subunit to form a stable heterodimer.[31] Recombinant Leu234Ile RT enzyme is 22-fold less sensitive to S-1153 than wild type, the most resistant single mutation against this drug. However, the Leu234Ile resistance mutation has only been observed as a part of a triple mutation with Lys103Thr and Val106Ala after prolonged selection pressure from S-1153.[36] These observations can be interpreted as evidence of the lower propensity of Leu234 to mutate under drug selection pressure than many other residues surrounding the NNRTI pocket. In addition to the lower propensity of residues associated with the 'primer grip' to mutate under selection pressure, residue Tyr318 appears to be generally highly conserved, there is only one report of Tyr318 being mutated (Tyr318Phe) in patients treated with NNRTIs, where resistance to delavirdine was shown.[45] Site-directed mutatagenesis of residue 318 to either Cys, Leu, Lys or His drastically reduced RT activity to only 5% of wild type.[46] Only conservative mutations of Tyr318 to Phe and Trp significantly retained enzyme activity (95% and 54% of wild-type activity, respectively). These mutagenesis experiments demonstrate the importance of Tyr318 in HIV-1 RT. In the both unliganded and NNRTI bound structures of RT the hydroxyl group of the Tyr318 phenol side chain forms a hydrogen bond to the main chain nitrogen of His235.[6,7] This bond links the connection domain and the palm domain and may be important in forming the correct conformation of the enzyme in this region.

The discrepancy between the large variety of drug resistant mutations reported in vitro and the far more limited set of clinically observed resistance mutants can be explained if one considers the tradeoff relationship between drug resistance and enzymatic, and thus viral, fitness. The widespread occurrence of Tyr181Cys and Lys103Asn mutations in clinical use of NNRTIs is most likely due to the ability of these specific mutations to provide resistance without severely affecting enzyme efficiency and hence viral replication. The limitations on the repertoire of resistance mutations used by the virus resulting from structural and fitness constraints lead to a balance between resistance/fitness which can provide an opportunity to devise design strategies which takes these factors into account. In the next section we attempt to apply the knowledge of structural constraints to the design a series of NNRTIs with improved activity against common drug resistant strains.

Structure-Based Design. A plausible strategy, to improve the performance of an NNRTI against the known drug resistant mutations, would be to target the inhibitor to make strong interactions with the conserved regions in the pocket, such as main chain atoms and the conserved residues while decrease the dependence on interactions with the mutable residues. In addition to the rapid selection of drug resistance, a further difficulty facing the rational design of an NNRTI is the observed plasticity of the binding site inherent in the structure, since this is an allosteric binding pocket formed upon binding the inhibitor. The size and volume of the NNRTI pocket, is greatly affected by the movement of the Pro236 hairpin loop and the repositioning of β10 strand (residues 232−234) and β11 strand (residues 239−241). Although the Pro236 loop occupies a fan of positions that track the size of the various NNRTIs, each can be classified into two discrete binding modes. The first mode is a nevirapine-type binding pocket observed for the binding of small NNRTIs to RT (such as nevirapine,[6] 9-Cl-TIBO,[47] α-APA[6] and 1051U91[6]). The nevirapine-type NNRTI pocket is defined by a hydrogen bond between the main chain nitrogen of Lys103 and the main chain carbonyl oxygen of Pro236. This hydrogen bond is formed when the flexible Pro236 hairpin loop moves about 5 Å, to encapsulate a small NNRTI. In a second binding mode the NNRTI pocket appears able to adopt is a BHAP-type pocket. On binding of larger NNRTIs, such as BHAP[9] or HEPT analogues[8,43] the Pro236 hairpin loop is closer to the *apo* conformation, forming a more open pocket in which there is no hydrogen bond between Lys103 and Pro236.

The open conformation of the BHAP-type pockets exposes the peptide backbone of Lys103 enabling the possibility of forming a series of hydrogen bonds to the main chain atoms of residues Lys101 to Lys103. Previously we have discussed the possible advantages of an inhibitor mimicking a peptide β-sheet binding to the conserved main chain residues. However, the difficulties of accurately exploiting main chain interactions with hydrophilic groups by design lead us to avoid this approach.[48] However, after our undertaking this current work, our group has elucidated the crystal structure of RT complexed with S-1153, which fortuitously fulfils our earlier prediction that, providing there is little depen-

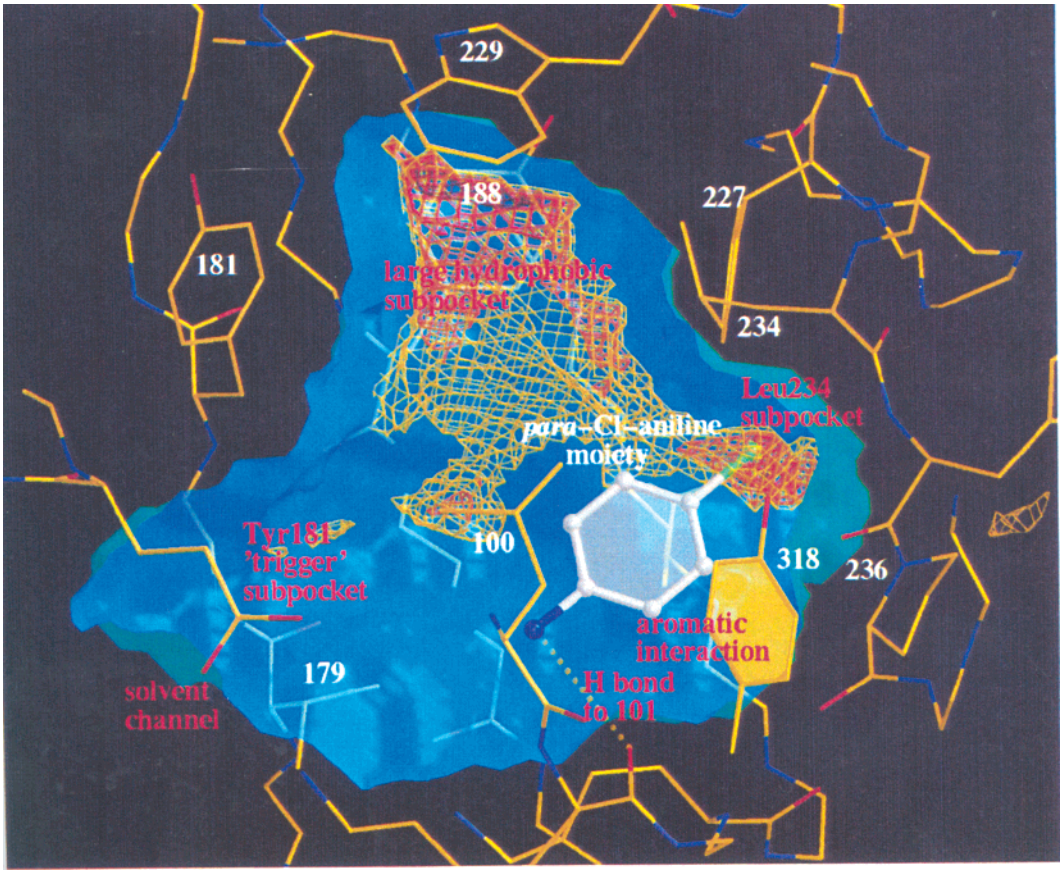

Figure 2. Exploiting contacts to the conserved regions. The *p*-chloroaniline moiety (grey − carbon atoms; blue − amine nitrogen; green − chlorine atom) makes good contacts to the conserved region of the NNRTI pocket. The benzyl ring is positioned to exploit aromatic interactions with Tyr318. The amine nitrogen can form a hydrogen bond to the carbonyl oxygen of Lys101 and the chloro group fits snugly into the Leu234 subpocket. The surrounding protein is shown as thin sticks (yellow − carbon atoms; red − oxygen; blue − nitrogen). The solvent-accessible surface is colored blue (calculated using the program VOLUMES calculated by rolling a 1.4 Å probe over the surface of the protein structure (R. Esnouf, unpublished)). The energy contour levels for the hydrophobic probe (calculated using the program GRID[53]) are contoured at: −0.5 kcal mol^{-1} (yellow); −1.0 kcal mol^{-1} (orange); −1.5 kcal mol^{-1} (red); −2.0 kcal mol^{-1} (brown).

dency on interactions with the side chain of Pro236, forming a large number of van der Waals and hydrogen bonding interactions of the Lys101-Lys103 backbone may significantly improve the resistance profile of NNRTIs.[49]

The smaller, encapsulated nevirapine-type pocket also provides opportunity for interactions with conserved residues. The movement of Pro236, enclosing the pocket, causes the side chains of residues Pro236, Pro225, Phe227, Leu234 and the main chains of His235 and Pro236 to partially collapse and form a compact subpocket, henceforth known as the 'Leu234 subpocket'. The Leu234 subpocket appears hydrophobic in nature and is surrounded by a cluster of residues, which have not been observed as primary resistance mutations and is flanked by the conserved residue Tyr318. We judged for the purpose of a structure-based design exercise that the exploitation of contacts to the more conserved residues, Trp229, Leu234 and Tyr318, could be best accomplished by designing inhibitors to fit into the small nevirapine-type pockets and interact with the compact Leu234 subpocket.

The inhibitor design strategy in this current work involved determining which moieties and groups would provide the best complementarity to each of the individual subpockets in the NNRTI binding site and connecting the groups together in a scaffold which would prove synthetically accessible. Hydrophobicity is a key feature driving the potency of inhibitor binding to the NNRTI site, and thus identification of hydrophobic binding sites is an important consideration in the design of NNRTIs. Analysis of the NNRTI site (see Experimental Section) reveals the deepest hydrophobic minimum occurs in the upper part of the pocket near to residue Trp229 and the second deepest in the Leu234 subpocket (Figure 2). These two minima are found in a general hydrophobic space connecting the Leu234 subpocket with the upper hydrophobic pocket along residues His235, Leu234, Phe227, Tyr188, Trp229, Tyr181 and Val106. In contrast, the GRID water and NH amine hydrophilic probes suggest there are relatively few opportunities for hydrogen bonds inside the NNRTI binding pocket. The hydrophilic region of the pocket is situated along the peptide backbone of residues Lys103 and Lys101 and into the solvent channel past residue Glu138 (p51). Both the water and the NH amine probes indicate that strong hydrogen bonds can be formed to the carbonyl oxygen of Lys101. Crystallographic observations and GRID calculations confirm the strong potential to form a hydrogen bond with the main chain carbonyl oxygen of Lys101. A nitrogen atom was therefore placed at a distance of 3.0 Å from the main chain carbonyl oxygen of Lys101, in a similar position to the 3-NH of the pyrimidine rings of the HEPT analogues to exploit this

anchor point. Exploitation of van der Waals contacts to the hydrophobic and conserved Leu234 subpocket and the aromatic character of the Tyr318 could provide valuable interactions between the inhibitor and the more conserved region of the NNRTI pocket. The putative inhibitor was based on a benzene ring exploiting aromatic $\pi-\pi$ interactions with residue Tyr318. A benzene ring was placed in an off-center stacking position relative to the ring plane of Tyr318, with a centroid-centroid distance of 4.5 Å between the two aromatic rings. A small hydrophobic subpocket exists in the NNRTI binding site next to Leu234. Exploitation of the pocket by a tight fitting group, such as a chloro, bromo, methoxy, methyl or nitrile, could make numerous van der Waals interactions with the side chains of Phe227 and Leu234 and the main chain atoms of His235 and Pro236. These three putative interactions with the Lys101 main chain, the Tyr318 aromatic ring and the Leu234 subpocket can be connected to form a *p*-chloroaniline moiety (Figure 2). Interestingly many chemically diverse second generation NNRTIs, such as efavirenz, HBY-097, UC-781 and PETT-2 contain this *para*-chloroaniline motif.

The upper part of the NNRTI binding site is a large cavity, predominately of aromatic character, formed by Tyr181, Tyr188, Phe227 and roofed by Trp229. Previously we have argued that the $\pi-\pi$ aromatic interactions which may be beneficial in the wild-type pocket may be unfavorable in the Tyr181Cys mutant pocket.[8] Ideally substitutents in the upper part of the NNRTI pocket should maximize contacts with the conserved residue Trp229 while avoiding the energetic complication of differing aromatic stacking environments between wild type and reducing the overall percentage of contacts with the mutable residues Tyr181 and Tyr188. Our previous studies on HEPT analogues has already demonstrated that by positioning a cyclohexyl group in the upper part of the NNRTI pocket an inhibitor can utilize this region of the pocket for both the wild type and Tyr181Cys mutant.[43]

A final key aspect of the compound design is the provision of a substituent to occupy the subpocket at the base of the Tyr181 side chain. Analysis of the structures of RT complexed with HEPT analogues lead to the hypothesis that a potent inhibitor should have a substituent that fills the volume of the small Tyr181 subpocket, situated between the side chains of Val179 and Tyr181 and walled by the main chain atoms of residues 180 and 181. Small hydrophobic groups such as ethyl, propyl or isopropyl provide substitutents of the correct size.

After several iterative design rounds (following the procedures outlined in the Experimental Section) involving building and evaluating a variety of distinct chemical scaffolds, the final selection of quinolone analogues was determined as a compromise between the design principles outlined above and synthetic accessibility (Figure 3). Given the promiscuity of the NNRTI binding site a wide variety of other compounds could be designed followed the criteria outlines above. To test the hypothesis that knowledge gained from the structural analysis of the mechanisms of RT inhibition and drug resistance can guide the design of improved 'second

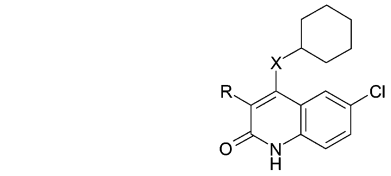

R = Pr, *i*-Pr
X = O, S, SO

No.	R	X
2a	Pr	O
2b	*i*-Pr	O
5	Pr	S
6	Pr	SO

Figure 3. Proposed quinolone-based non-nucleoside inhibitors of HIV-1 RT.

Scheme 1. Synthesis of 6-Chloro-4-cyclohexyloxy-3-propylquinol-2-one (**2a**, R = Pr)). Replacement of the Diethyl Propylmalonate with Diethyl Isopropylmalonate in the First Step Led to the Synthesis of **2b** (R = *i*-Pr)

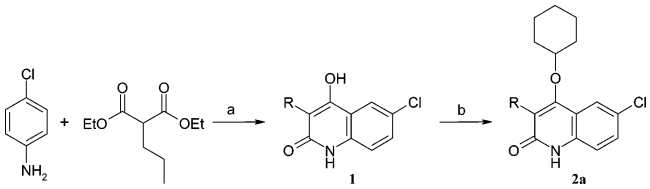

[a] Reagent and conditions: (a) Ph_2O, N_2, 250 °C reflux, 20 h; (b) bromocyclohexane, DMF, Et_3N, K_2CO_3, N_2, 21 h reflux.

generation' inhibitors the quinolone analogues were synthesized and evaluated.

Chemistry. The synthesis of the 4-alkyloxyquinolones and 4-alkylthioquinolones compounds was accomplished separately using two distinct synthetic schemes from 4-hydroxyquinol-2-ones intermediates. The general procedure to form 4-hydroxyquinol-2-ones is by the reaction of the diethyl malonate ester with aniline to form the malonanilide with the liberation of ethanol. The ring closure of the malonanilide and tautomerization leads to the formation of the common intermediate 4-hydroxyquinol-2-one (**1**).

The complete syntheses of the alkyloxy quinolone ethers, compounds **2a** and **2b**, are two-step processes (Scheme 1). Scheme 1 enables the simple substitution of groups at positions 3 and 6 on the quinolone, but is limited to the synthesis of alkyloxy quinolone ethers only. 4-Hydroxyquinol-2-ones (compounds **1a** and **1b**) were heated with an alkyl bromide (cyclohexyl bromide) under basic conditions (potassium carbonate and triethylamine) to form 4-cyclohexyloxyquinol-2-ones via the Williamson synthesis of an unsymmetrical ether.

Scheme 2 provides a general method for synthesising unsymmetrical ethers or thioethers, with any alkyloxy, alkylthio, and aryloxy or arylthio substituents to the 4-position of the quinolone. The 4-hydoxy-quinol-2-one (**1**) is brominated[50] with heated phosphorus tribromide to produce the 2,4-dibromoquinoline compound (**3**). Hydrolysis of compound **3** to the 4-bromo-1*H*-quinol-2-one (**4**) was achieved by heating in glacial acetic acid containing a small amount of water. The displacement of the bromide in compound **4** by the sodium mercaptan salt (prepared in situ) leads to the formation of the 4-cyclohexylthioquinol-2-one (**5**). Oxidation of the sulfur, in compound **5**, with *m*-chloroperbenzoic acid (MCPBA) led to the formation of the sulfinyl derivative (**6**). Details of the all the reactions are given in the Experimental Section.

Scheme 2. Synthesis of 6-Chloro-4-cyclohexylthio-3-propylquinol-2-one (**5**) (**a**, R = Pr; **b**, *i*-Pr)

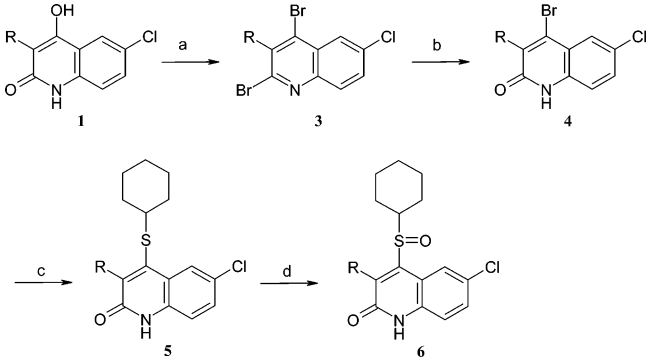

[a] Reagents and conditions: (a) PBr_3, 140 °C, reflux, 4.5 h; (b) acetic acid, water, 125 °C reflux, 8 h; (c) dry DMF, N_2, 20 h, 140 °C, sodium cyclohexane mercaptan; (d) MCBPA, room temperature, 1 h.

Table 1. Inhibition of Wild-Type and Mutant HIV-1 RT by Quinolone Compounds. Data Are the Mean Value of Two Independent Experiments

compd	wild-type RT IC_{50}, μM	Cys181 RT IC_{50}, μM (*fold*)[a]	Ile100 RT IC_{50}, μM (*fold*)[a]
2a	0.71	1.13 *(1.5)*	1.36 *(1.9)*
2b	0.63	2.50 *(3.9)*	1.96 *(3.1)*
5	0.24	0.86 *(3.6)*	1.61 *(6.7)*
6	0.38	1.26 *(3.3)*	2.38 *(6.2)*
nevirapine	0.30	>100 *(>100)*	>100 *(>100)*

[a] Multiple fold increase in IC_{50} between wild-type and mutant HIV-1 RT.

Results

All four of the lead quinolone compounds tested (**2a**, **2b**, **5** and **6**) proved to be potent and selective inhibitors of HIV-1 RT (Table 1). The comparison with nevirapine starkly shows the success of the designed quinolone compounds in inhibiting the common drug resistant RT mutants, Tyr181Cys and Leu100Ile. Whereas the sensitivity of the mutant enzyme to nevirapine is reduced more that 100 fold, the quinolone compounds, as a series, show decreases between 1.5- and 7-fold. The average increase in the IC_{50} values for the four inhibitors against the Cys181 and Ile100 mutant RTs was only a 3.1-fold and 4.5-fold, respectively. The most potent inhibitor of the Cys181 mutant RT is, again, compound **5**, with an IC_{50} = 0.86 μM, while the most potent inhibitor of the Leu100Ile mutant is compound **2a** (IC_{50} = 1.36 μM). The 4-cyclohexyloxyquinolone analogue, **2a**, is the least affected by the resistance mutations as indicated by only a 1.5-fold increase in IC_{50} against the Tyr181Cys mutant and only 1.9-fold increase for Leu100Ile, when compared to the IC_{50} for wild-type RT. The quinolone compounds (**2a**, **2b**, **5** and **6**) are demonstrated to be potent inhibitors of wild-type ($HIV\text{-}1_{IIIB}$) and nevirapine-resistant strains of HIV-1, in the MT4 cell assay (Table 2). The 4-cyclohexyloxy quinolone derivatives, **2a** and **2b**, are extremely potent inhibitors of HIV-1, with IC_{50} = 35 nM and IC_{50} = 51 nM, respectively. The 4-cyclohexylthioquinolone derivative, **5**, appears to be least affected by the Tyr181Cys mutation in the nevirapine-resistant HIV-1 strain, with an IC_{50} = 0.368 μM which is only an increase of 3.6-fold over the inhibition value for wild type. The sulfinyl analogue, **6**, displays the least impressive performance of the four compounds, with significantly higher 50% inhibition concentrations for both wild-type and nevirapine-resistant HIV-1, relative to the other three.

Table 2. Antiviral Activity of Quinolone Inhibitors in MT4 Cells

compd	$HIV\text{-}1_{IIIB}$ [a] IC_{50}	nevirapine-resistant HIV-1[b] IC_{50} (*fold*)[c]
2a	0.035	0.607 *(17)*
2b	0.051	0.710 *(14)*
5	0.100	0.368 *(4)*
6	0.242	2.210 *(9)*

[a] $HIV\text{-}1_{IIIB}$ virus [b] HIV-1 virus containing Tyr181Cys mutation in RT. [c] Multiple increase in IC_{50} between wild-type (IIIB) and nevirapine-resistant HIV-1 strains.

To confirm if the quinolones bound to RT as predicted, the actual binding mode of the compounds were observed by determination of the X-ray crystallographic structures of the four quinolone analogues, **2a**, **2b**, **5** and **6** complexed with HIV-1 reverse transcriptase. Details of the crystallization and structure determinations of the four RT−inhibitor complexes are outlined in the Experimental Section. The overall structures of the RT−quinolone complexes have the same general description of the RT p66/p51 heterodimer as reported for the other RT−NNRTI complexes and show no significant global rearrangements. The electron-density maps clearly and unambiguously show the positions, orientations and conformations of the inhibitors bound at the NNRTI site (Figure 4). The $|F_{obsd}| - |F_{calcd}|$ omit map for RT−**6** (Figure 4d) indicates the chirality of the sulfinyl compound is modeled as the *R* enantiomer. The protein−inhibitor interactions for the structures of the quinolones compounds complexed to RT are very similar for all four complexes. Comparison of the binding of the quinolone inhibitors to RT between the crystal structures and the modeled structures reveal an extremely close overlap (mean rms deviation between the crystal structures and the models is 0.5 Å).

A strong hydrogen bond between the N1H of the heterocylic ring of the quinolone moiety and the main chain carbonyl oxygen of Lys101 is observed, as predicted. Water has only been built into the 2.6 Å resolution map of the RT−**2a** complex. In this complex the inhibitor is orientated into position by an additional hydrogen bond between the carbonyl oxygen O2 of the quinolone and a water molecule, which in turn forms a hydrogen bond to the side chain of Lys103 (Figure 1). This water molecule is situated in the channel that leads to the bulk solvent but makes different hydrogen bonds to the equivalent water molecule in the RT−MKC-442 and related structures, which bond to the side chains of Glu138(p51) and Lys101. Although no water molecules have been modeled into the electron density maps of the other three structures, the conformation of the Lys103 side chains and the position of the O2 carbonyl oxygen of the quinolones are such that water could hydrogen bond in the same position as in the RT−**2a** model.

The position of the Pro236 loop is the same in all four of the RT−inhibitor complexes and closely resembles the position of Pro236 in the RT−TIBO complex, the reference structure used for the initial inhibitor design. The quinolone moiety of the inhibitors sits between the hydrophobic residues Val106 and Leu100 and is flanked by Tyr318. The quinolone group of all four inhibitors is in the same plane, with the benzene ring moiety

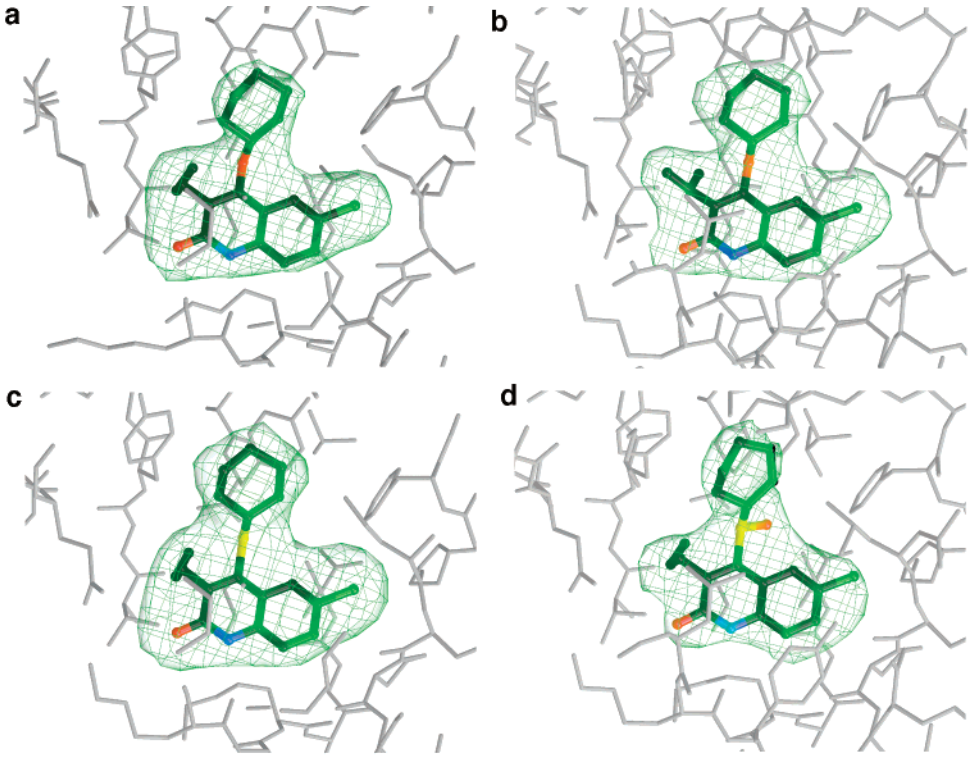

Figure 4. Diagrams of the electron density omit $|F_{obsd}| - |F_{calcd}|$ maps contoured at 3σ of the quinolone inhibitors bound at the NNRTI binding site of HIV-1 RT for (a) RT−**2a**, (b) RT−**2b**, (c) RT−**5** and (d) RT−**6** complexes. The inhibitors are shown as ball-and-stick representations where the atoms are colored by type (grey − carbon; red − oxygen; blue − nitrogen; green − chlorine; yellow − sulfur) and the surrounding protein is displayed as gray sticks. The omit maps are shown as green nets.

appearing to interact with the conserved residue Tyr318 by aromatic−aromatic, off-center π-stacking,[51] there is an average centroid to centroid distance of 4.5 Å between the ring planes. The 7-chloro substituents of the quinolones fit snugly into a subpocket created by the encapsulating movement of the Pro236 hairpin loop. The 7-chloro substituents form close van der Waals (≤3.7 Å Cl−C van der Waals contacts) to the surrounding residues Phe227, Leu234, His235, Pro236, side chain and main chain atoms. The 3-propyl groups of **2a**, **5** and **6** extend to fill the subpocket at the main chain Tyr181 and side chain of Val179. The terminal methyl of the 3-propyl group makes close contacts to main chain atoms of Tyr181 and Tyr188 and the side chain of Val179. The shorter 3-isopropyl group of **2b** would still clash with the *apo* conformation of Tyr181, but makes less of a intrusion into this subpocket, making contacts to Tyr188, since both the 3-isopropyl and 3-propyl quinolone analogues are in the same plane. **2b** does not rearrange its orientation in the pocket to place the 3-isopropyl deeper into the Tyr181 subpocket. The main differences between the four RT−quinolone complexes are the subtle changes in the position and interactions of the 4-cyclohexyloxy and 4-cyclohexylthio substituents with the protein. The cyclohexyl ring of all the inhibitors sits in the upper part of the NNRTI binding site, which is mainly aromatic in character, surrounded by residues Leu100, Tyr181, Tyr188, Phe227 and Trp229, the latter lying at the top of the pocket, close to normal to the plane of the tyrosine side-chains and cyclohexyl group. The cyclohexyl ring in all four inhibitors adopts the same chair conformation. Due to the longer carbon−sulfur bond length and sharper bond angle the 4-cyclohexylthio substituent fits slightly deeper into the pocket, enabling closer contacts to the conserved residue Trp229. The increased hydrophobic character of the thioether linker in **5** as compared with the oxy ether linker of **2a** and **2b** and the deeper penetration into the hydrophobic pocket may account for the lower IC_{50} of **5** against RT enzyme than **2a** and **2b**.

Conclusion

A detailed analysis of both the structure of the NNRTI pocket and the available data on drug resistance for this compound class led to a structure-based design approach to the synthesis of novel inhibitors of HIV-1 RT. For reasons of synthetic accessibility, we decide to focus our chemistry efforts on the quinolone scaffold, yet we believe the general strategies, outline here, for tackling drug resistance can be applied as design principles to the search for other NNRTI chemotypes. These initial results indicate the quinolone series was much more favorable than nevirapine when comparing inhibition of the clinically important Tyr181Cys mutation in HIV-1 RT. These initial results provided us with enough confidence to extend this study to further explore the potential of this approach in the design of further analogues in the quinolone series of NNRTIs. In Part 2 of this work we provide further evidence from the comprehensive screening of quinolone analogues against a broad panel of HIV-1 RT drug resistance mutants for the potential of this series and this approach in the design of NNRTIs with improved drug resistance profiles.[52]

Experimental Section

Computational Chemistry. Iterative rounds of compound design and retrosynthetic analysis were conducted in the following manner. The NNRTI binding pocket was defined by

calculating a solvent accessible surface using the program VOLUMES (Dr. R. Esnouf, unpublished). The energy contours for the hydrophobic and hydrophilic probes were calculated using the program GRID (version 14).[53] Molecules expected to fulfill the design criteria were constructed and minimized using the program SYBYL (Tripos Associates) on an R10000 Silicon Graphics workstation. The molecules were initially manually docked into the NNRTI binding site of the RT model guided by superposition models of the all the available RT−inhibitors structures, using the protein model of the RT−9-Cl-TIBO as the main reference structure (2.6 Å resolution; PDB accession number 1REV[47]). The position of the docked molecules were refined in the NNRTI pocket were subject to energy minimization using the conjugate gradient method[54] as implemented in X-PLOR[55] with the protein fully restrained. Protein−inhibitor interactions were calculated using X-PLOR. The synthetic accessibilities of the molecular designs were evaluated by searching the synthetic reaction database at Daresbury Laboratory.[56]

Synthetic Chemistry. ^{1}H NMR spectra were obtained on a Brücker AC250 (200 MHz) spectrometer, DMSO-d_6 and $CDCl_3$ were used as solvents, with tetramethylsilane (TMS) added as an internal standard in all cases. Data are reported as follows: chemical shifts reported in ppm units relative to the TMS internal reference, multiplicity (b = broad, s = singlet, d = doublet, t = triplet, m = multiplet, q = quartet), coupling constant (Hz), integration and chemical group. LC-MS (liquid chromatography−mass spectrometry) data were collected on a Hewlett-Packard spectrometer. All compounds were routinely checked by ^{1}H NMR, LC-MS and TLC. NMR spectral data were consistent with the indicated structures and LC-MS data were consistent with expected masses. Reactions were monitored by thin-layer chromatography, on glass plates coated with silica gel and visualized by UV light. Elemental analyses were determined by Butterworth Laboratories Ltd. IR spectra were recorded on a Biorad FT-IR FTS155 spectrophotomer with compounds pressed into KBr pellets. Melting points were measured in open capillary tubes using a Büchi melting point apparatus and are uncorrected. Separations by flash chromatography were performed with Merck silica gel (Merck No. 60, 230-400 Mesh). All reagents and solvents were of commercial quality. Solvents were dried using standard procedures. Concentrations of solutions after reactions and extractions involved the use of a rotary evaporator operating at a reduced pressure of approximately 15 Torr. Organic solutions were dried over sodium sulfate. Samples prepared for physical data and biological testing were dried overnight under high vacuum.

6-Chloro-4-hydroxy-3-propyl-1*H*-quinol-2-one (compound 1a). 4-Chloroaniline (10 g: 0.08mol) and diethyl propylmalonate (16.31 mL; 0.08mol) were dissolved in diphenyl ether (100 mL). The reaction mixture was heated to reflux at 250 °C in a liquid metal bath and stirred. The reaction was conducted under a nitrogen atmosphere with the nitrogen blowing onto the surface of the reaction solution. After 20 h the reaction was cooled. The reaction flask was placed in a 50 °C water bath to prevent the diphenyl ether from solidifying. Colorless crystals of the product crystallized out of the warm solution. These crystals were filtered off, washed with light petroleum ether (bp 40−60 °C) and dried in a vacuum over for several hours to give 11.63 g of pure product: Yield 61.3%. Melting point of white crystals, 245 °C. ^{1}H NMR 200 MHz (DMSO-d_6) 11.44 (s, 1H, NH), 10.25 (s, 1H, OH), 7.85 (s, 1H, 5-H), 7.49 (d, J = 5 Hz, 1H, 7-H), 7.25 (d, J = 5 Hz, 1H, 8-H), 2.52 (t, J = 5 Hz, 2H, propyl 2′-H_2), 1.45 (m, 2H, J = 5 Hz, propyl 1′-CH_2), 0.9 (t, J = 5 Hz, 3H, propyl 3′-H_3). Anal. ($C_{12}H_{12}NO_2Cl$) C, H, N.

6-Chloro-4-hydroxy-3-isopropyl-1*H*-quinol-2-one (compound 1b). 4-Chloroaniline (10 g; 0.08mol) and diethyl isopropylmalonate (0.08mol; 16.1 g) were dissolved, by stirring, into diphenyl ether (70 mL). The reaction mixture was heated to 250 °C and refluxed, under a stream of nitrogen, for 24 h. On cooling to 50 °C a white solid precipitated out of the reaction solution. The solid product was filtered off, washed with light petroleum ether and dried to give pure product (12.16 g; 0.051mol). Yield 63.8%. R_f product = 0.1 (10% EtOAc/90% hexane). Melting point of product, 255−256°C. ^{1}H NMR 200 MHz (DMSO-d_6) 11.35 (s, 1H, NH), 10.10 (s, 1H, OH), 7.9 (s, 1H, 5-H), 7.45 (d, J = 5 Hz, 1H, 7-H), 7.24 (d, J = 6.5 Hz, 1H, 8-H), 3.4 (m, 1H, *i*-propyl 1′-H), 1.28 (d, J = 5 Hz, 6H, *i*-propyl 2′,3′-H). Anal. ($C_{12}H_{12}NO_2Cl$) C, H, N.

6-Chloro-4-cyclohexyloxy-3-propyl-1*H*-quinol-2-one (compound 2a). 6-Chloro-4-hydroxy-3-propyl-1*H*-quinol-2-one (0.5 g; 2.1 mmol) was dissolved in DMF (50 mL). To this solution was added 2 equiv of cyclohexyl bromide (0.52 mL; 4.2 mmol), 1.1 equiv of potassium carbonate (0.319 g; 2.31 mmol) and triethylamine (0.21 mL). The reaction mixture was heated to 140 °C, under a nitrogen atmosphere, overnight. LC-MS after this time indicated that about 30% of the starting material had been converted to product. The mixture was allowed to cool and filtered to remove insoluble potassium carbonate. Volatiles were removed in vacuo. The remaining dark red solid was dissolved in DCM (100 mL) and washed with water and then brine. The organic layer was dried by adding solid anhydrous sodium sulfate. The crude product was concentrated to a solid by removing the organic solvent under reduced pressure. The crude dark red solid was dissolved in a minimum amount of ethyl acetate with a small addition of acetone to aid solubility. The final product was isolated and purified by silica column chromatography (solvent system initially 100% hexane, slowly increasing the concentration of ethyl acetate). The fractions containing the product were pooled and volatiles removed in vacuo to recover 53 mg amorphous solid of pure product: Yield 8%. Melting point of solid product 214−215 °C. ^{1}H NMR 200 MHz ($CDCl_3$) 12.0 (s, 1H, NH), 7.75 (s, 1H, 5-H), 7.4 (d, J = 5 Hz, 1H, 7-H), 7.3 (d, J = 10 Hz, 1H, 8-H), 4.1 (m, 1H cyclohexyloxy OCH), 2.7 (t, J = 5 Hz, 2H, propyl 1′-H), 2.08 (m, 2H, C_{2ax}, C_{6ax} cyclohexyl-H), 1.85 (m, 2H, C_{2eq}, C_{6eq} cyclohexyl-H), 1.67 (m, 2H, propyl 2′-H), 1.28 (m, 6H, C_4, C_5, C_6 cyclohexyl-H), 1.03 (t, J = 5 Hz, 3H, propyl 3′-H). Anal. ($C_{18}H_{22}NO_2Cl$) C, H, N.

6-Chloro-4-cyclohexyloxy-3-isopropylquinol-2-one (compound 2b). 6-Chloro-4-cyclohexyloxy-3-isopropyl-quinol-2-one (0.5 g) was dissolved in dry DMF (50 mL). To this solution was added triethylamine (0.45 mL), potassium carbonate (1 g) and 5 equiv of cyclohexyl bromide. The reaction mixture was stirred and heated to 150 °C for 48 h. On cooling the reaction mixture was filtered and volatiles were removed in vacuo. The remaining residue was dissolved into 5 mL of ethyl acetate. The product was obtained by silica column chromatography (initial column 100% hexane, increasing the concentration of ethyl acetate, $R_f^{product}$ = 0.1 (10% ethyl acetate/90% hexane)) to give 50 mg of product. Yield 8%. Melting point of solid product 190−191 °C. ^{1}H NMR 200 MHz ($CDCl_3$) 12.4 (s, 1H, NH), 7.75 (s, 1H, 5-H), 7.4 (d, J = 7.5 Hz, 1H, 7-H), 7.3 (d, J = 6 Hz, 1H, 8-H), 4.03 (m, 1H, cylcohexyloxy OCH), 3.45 (m, 1H, *i*-propyl C_1H_1), 2.08 (m, 2H, cyclohexyl-H C_{2ax}, C_{6ax}), 1.85 (m, 2H, cyclohexyl C_{2eq}, C_{6eq}), 1.52−1.75 (m, 6H, cyclohexyl-H, C_3, C_4, C_5), 1.48 (d, J = 5 Hz, 6H, *i*-propyl C_2-H_3, C_3-H_3). Anal. ($C_{18}H_{22}NO_2Cl$) C, H, N.

2,4-Dibromo-6-chloro-3-propylquinoline (compound 3). 6-Chloro-4-hydroxy-2-quinolone (3.0363 g; 0.013 mol) was mixed with phosphorus tribromide (50 mL). The reaction mixture was stirred and heated to 140 °C. The crust that formed on top of the reaction mixture was broken up at intervals. After 4.5 h the mixture was cooled, poured into iced water (500 mL) and left to stand overnight. The crude product (3.57 g) was collected and crystallized from 95% ethanol to give white, slender, needle crystals of pure product (800 mg). Yield 17%. Melting point of crystals 109−110 °C. ^{1}H NMR (DMSO-d_6) 8.15 (s, 1H, 5-H), 8.05 (d, J = 7.5 Hz, 1H, 7-H), 7.88 (d, J = 7.5 Hz, 1H, 8-H), 3.1 (t, J = 5 Hz, 2H, propyl 1′-CH_2), 1.65 (m, 2H, propyl 2′-CH_2), 1.05 (t, J = 5 Hz, 3H, propyl 3′-CH_3). Anal. ($C_{12}H_{10}NClBr_2$) C, H, N.

4-Bromo-6-chloro-3-propyl-1*H*-quinol-2-one (compound 4). The 2,4-dibromoquinoline analogue (compound 3, 100 mg; 0.275 mmol) was mixed with a solution of glacial acetic acid

(10 mL) and water (5 mL). The reaction mixture was heated to 125 °C and refluxed for 8 h. On cooling a white solid precipitated from the solution, which was collected and dried to give pure product (80 mg; 97.5% yield). Melting point of product 216−217 °C. ^{1}H NMR ($CDCl_3$) 11.45 (s, 1H, NH), 8.0 (s, 1H, 5-H), 7.45 (d, J = 5 Hz, 1H, 7-H), 7.23 (d, J = 5 Hz, 1H, 8-H), 2.92 (t, J = 5 Hz, 2H, propyl 1′-CH_2), 1.66 (m, 2H, propyl 2′-CH_2), 1.05 (t, J = 4 Hz, 3H, propyl, 3′-CH_3). Anal. ($C_{12}H_{11}NOClBr$) C, H, N.

6-Chloro-4-Cyclohexylthio-3-propyl-1*H*-quinol-2-one (compound 5). Sodium hydride (60% oil dispersion, 4 mmol; 0.16 g; 4 equiv) was mixed with cyclohexyl mercaptan (8 mmol; 0.98 mL; 8 equiv) in dry DMF (5 mL) at 0 °C for 45 min. Solid 4-bromo-quinol-2-one compound (300 mg; 0.001mol) was dissolved into dry DMF (5 mL) and added to the sodium cyclohexyl mecaptan salt. The reaction mixture was heated to 140 °C, under a nitrogen atmosphere, for 20 h. On cooling, a solid white precipitate was filtered off and volatiles removed in vacuo. The remaining solid was dissolved in ethyl acetate (40 mL). On addition of a small amount of water (10 mL) to wash the organic layer, a white precipitate was produced. The solution was gently heated to redissolve the white precipitate. The water layer was removed by use of a separating funnel and the remaining organic layer dried with solid anhydrous sodium sulfate. Volatiles were removed in vacuo, and the product was recrystallized from ethyl acetate to give white crystals of pure product (209 mg; yield 62%). Melting point of white crystals 246−247 °C. ^{1}H NMR 200 MHz ($CDCl_3$) δ 10.89 (s, 1H, NH), δ 8.21 (s, 1H, 5-H), δ 7.41 (d, J = 5 Hz, 1H, 7-H), δ 7.20 (d, J = 5 Hz, 1H, 8-H), δ 3.05 (t, J = 5 Hz, 2H, propyl 1′-CH_2), δ 3.0 (m, 1H, cyclohexylthio SCH), δ 1.9 (m, 2H, cyclohexyl C_{2ax}, C_{6ax}), δ 1.78 (m, 2H, cyclohexyl C_{2eq}, C_{6eq}), δ 1.57 (m, 2H, propyl 2′-CH_2), δ 1.25 (m, 6H, cyclohexyl C_3, C_4, C_5), δ 1.05 (t, J = 4 Hz, 3H, propyl 3′-CH_3). Structure confirmed by NOE of protons on C5 quinolone and C2 and C6 cyclohexyl. Anal. ($C_{18}H_{22}NOSCl$) C, H, N.

6-Chloro-4-(cyclohexylsulfinyl)-3-propyl-1*H*-quinol-2-one (compound 6). 4-Cyclohexylthioquinolone (**5**) (80 mg; 0.239 mmol) was dissolved in 10 mL of 2-propanol. To this solution was added 3-chloroperbenzoic acid (55% dispersion; 0.165 g; 0.526 mmol) mixed with 5 mL of 2-propanol. The reaction mixture was stirred for 1 h at room temperature, washed with saturated sodium hydrogencarbonate solution and dried over solid anhydrous sodium sulfate. The volume of 2-propanol was reduced in vacuo, gently heated and left to cool. Pure product was obtained from the solution in the form of white crystal (50 mg; yield 59.6%). Melting point of crystals 215−216 °C. ^{1}H NMR 200 MHz ($CDCl_3$) 11.3 (s, 1H, NH), 8.7 (s, 1H, 5-H), 7.5 (d, J = 5 Hz, 1H, 7-H), 7.28 (d, J = 5 Hz, 1H, 8-H), 3.45 (m, 1H, cyclohexyl SCH), 3.0 (m, 2H, propyl 1′-CH_2), 2.78 (m, 1H, cyclohexyl C_{2ax}, C_{6ax}), 2.45 (m, 1H, cyclohexyl C_{2eq} or C_{6eq}), 2.40 (m, 1H, cyclohexyl C_{2eq} or C_{6eq}), 2.03 (m, 1H, cyclohexyl C_{2eq} or C_{6eq}), 1.98 (m, 1H, cyclohexyl C_{2eq} or C_{6eq}), 1.58 (m, 2H, propyl 2′-CH_2), 1.45−1.20 (m, 6H, cyclohexyl-H C_3, C_4, C_5), 1.08 (t, J = 1m, 3H, propyl 3′-CH_3). IR ν 1049.16 (sulfoxide SO). Anal. ($C_{18}H_{22}NO_2SCl$) C, H, N.

Reverse Transcriptase Assay. Inhibition of recombinant HIV-1 reverse transcriptase was performed in a manner similar to previously published protocols[57,58] by determining the polymerase activity by measuring the incorporation of radiolabeled nucleotide into the primer DNA strand.

Antiviral Assay. The compounds were tested for their ability to inhibit wild-type HIV-1 (strain IIIB) and nevirapine-resistant HIV-1 (containing the Tyr181Cys mutation in the RT sequence). The activity of the compounds against HIV-1 in whole cell culture were measured using a propidium iodide-based colorimeteric assay, to estimate DNA content, in human T-cell lymphotropic virus-transformed cell line MT4 in a following previous reported protocols.[59−62]

Crystallization. Crystals of RT complexed with the quinolone compounds **2a**, **2b**, **5** and **6** were grown following the reported procedure.[63] Briefly, the crystals were grown by equilibration against reservoirs of 7−10% PEG 3350 and citrate−phosphate buffer (24.25 mM citric acid, 51.5 mM Na_2HPO_4) at pH 5, using the sitting drop method at 4 °C. Each drop containing 4 μL of enzyme−inhibitor solution and 4 μL of PEG/buffer mix and were microseeded using a light brush from a suspension of crushed RT−nevirapine crystals. The crystals were subject to partial dehydration by equilibrating with 50% PEG 3350 by gradually increasing the concentration of PEG over a period of 3 days.

X-ray Data Collection. Diffraction data for the RT−**2a**, RT−**2b** and RT−**5** complexes were collected on Station 7.2 at the SRS, Daresbury Laboratory, UK, using the oscillation method with X-rays of 1.488 Å wavelength collimated to a diameter of 200 μm. Data images of 1.5° oscillations were recorded using 120 s exposures on a 18 cm MAR Research imaging plate system which was positioned 130 mm from the crystal. Diffraction data from the RT−**6** complex were collected on beamline BM-14 at the ESRF, Grenoble, France, with X-rays of 0.918 Å wavelength using a 34.5 cm MAR Research imaging plate. All crystals were flash-frozen in liquid propane and maintained at 100 K in a stream of nitrogen gas, using an Oxford Cryosystems Cryostream (Long Hanborough, Oxon., UK). All datasets were collected from single crystals for each complex with negligible radiation damage.

Data images were auto-indexed and spot intensities were integrated using the program DENZO.[64] The observed data was corrected for Lorentz and polarization effects and reduced to a list of unique, indexed reflections with averaged intensities using the program SCALEPACK.[64] The orthorhombic crystals were in space group $P2_12_12_1$. From the cell parameters, all four of the complexes were classified as belonging to RT cell form F. Data collection and reduction statistics can be found in Table 3.

Structure Solution and Refinement. The RT−inhibitor complexes were solved by molecular replacement using X-PLOR.[55] All four of the structures were phased using the 2.6 Å resolution structure of the RT−9-Cl-TIBO complex[47] (excluding water and inhibitor molecules), which possesses a similar unit cell parameters (a = 138.8, b = 115.8, c = 66.2) to each of the complexes. Each of the data sets was separately refined by similar refinement protocols with CNS[65] using the Engh and Huber protein force-field parameters.[66] Initially, data from 10 to 6 Å resolution were used with the model as a single rigid body; then the p66 and p51 subunits were used as two rigid groups, and the nine domains in the heterodimer were each treated as separate rigid groups and refined initially against data from 10 to 4 Å resolution and finally against data from 10 Å to the high-resolution shell (2.6 Å for RT−**2a**, 2.8 Å for RT−**2b** and RT−**5** and 2.9 Å for RT−**6**).

Due to the low ratio of reflections to parameters, strong restraints on atom positions greater than 25 Å from the Cα atom of Tyr188 in the NNRTI binding site were employed in all subsequent refinements after the nine domain rigid body refinements. Each of the models from the rigid body refinement were subject to restrained positional refinement using data from 30−2.6 Å resolution, for the RT−**2a** complex, 30−2.8 Å for both the RT−**2b** and RT−**5** complexes and 25−2.9 Å for RT−**6**. To compensate for the weakness of the high-resolution reflections and the anisotropy in the data, each of the RT−quinolone complex datasets were sharpened using anisotropic B factor scaling against the structure factors calculated from a positional refined model where the atomic B factors were reduced. The sharpened datasets were used in further positional and restrained individual B factor refinement, incorporating a bulk solvent correction.

The $|F_{obsd}| - |F_{calcd}|$ difference maps for each of the RT−quinolone complexes clearly showed each of the inhibitors bound at their respective NNRTI binding site. Models of the complexes were built into the $2|F_{obsd}| - |F_{calcd}|$ and $|F_{obsd}| - |F_{calcd}|$ electron density maps using the program FRODO[67] on an Evans and Sutherland ESV workstation. The models were improved with iterative rounds of manual model building and positional refinement and restrained individual temperature factor refinements. All four of the structures have been assigned the secondary structure nomenclature as defined for

Table 3. Statistics for Crystallographic Structure Determinations

	RT−**2a**	RT−**2b**	RT−**5**	RT−**6**
	Data Collection Details			
data collection site	SRS PX7.2	SRS PX7.2	SRS PX7.2	ESRF BM-14
detector	MAR 18 cm	MAR 18 cm	MAR 18 cm	MAR 345 mm
wavelength (Å)	1.488	1.488	1.488	0.918
unit cell dimensions (*a, b, c* in Å)	138.3, 115.1, 65.2	138.0, 115.2, 65.3	137.8, 115.2, 65.0	137.5, 115.3, 65.4
resolution range (Å)	30.0−2.60	30.0−2.80	30.0−2.80	25.0−2.90
observations	73067	70383	65563	88607
unique reflections	28424	24466	24383	23603
completeness (%)	86.1	92.1	93.8	99.2
average $I/\sigma(I)$	9.5	9.8	9.2	19.8
R_{merge}[a]	0.087	0.103	0.104	0.052
	Outer Resolution Shell			
resolution range (Å)	2.69−2.60	2.90−2.80	2.90−2.80	2.97−2.90
unique reflections	2405	2186	2127	1460
completeness (%)	74.6	83.3	84.7	92.3
average $I/\sigma(I)$	1.2	1.6	1.4	2.5
	Refinement Statistics			
resolution range (Å)	30.0−2.60	30.0−2.80	30.0−2.80	25.0−2.90
no. of reflections(working/test)	27006/1380	23198/1171	23194/1169	22415/1135
R-factor[b] (R_{work}/R_{free})	0.209/0.282	0.205/0.286	0.206/0.281	0.221/0.282
R-factor[b] (all data)	0.200	0.197	0.200	0.218
no. atoms (protein/inhibitor/water)	7550/22/37	7576/22/−	7576/22/−	7567/23/−
rms bond length deviation (Å)	0.0114	0.0101	0.0101	0.0105
rms bond angle deviation (deg)	1.63	1.53	1.55	1.60
mean B-factor (Å^2)[c]	63/69/41/40	58/65/41/−	64/70/48/−	67/70/65/−
rms backbone B-factor deviation (Å^2)	3.8	3.5	3.6	3.6
PDB code	1TKT	1TL3	1TKZ	1TL1

[a] $R_{merge} = \Sigma|I - \langle I\rangle|/\Sigma\langle I\rangle$. [b] R-factor $= \Sigma|F_o - F_c|/\Sigma F_o$. [c] Mean B-factor for main-chain, side-chain, inhibitor and water molecules.

the RT−nevirapine structure.[6] Overall the electron density for each of the complexes was well defined, but a few small stretches of sequence were omitted from the models where the electron density maps showed disorder. Sections omitted from the models were as follows: RT−**2a** complex, residues 1−3, 64−70, 444−454, 538−560 from p66 and residues 1−6, 89−94, 214−224, 357−361, 428−440 from p51; RT−**2b** complex, residues 1−3, 64−69, 444−454, 538−560 from p66 and residues 1−6, 89−94, 215−224, 357−361, 428−440 from p51; RT−**5** complex, residues 1−3, 64−69, 444−454, 538−560 from p66 and residues 1−5, 89−94, 215−224, 357−361, 428−440 from p51; RT−**6** complex, residues 1−3, 64−69, 444−454, 538−560 from p66 and residues 1−6, 65−67, 89−94, 215−224, 357−361, 431−440 from p51. Water molecules were only incorporated into the high resolution, RT−**2a** model, in positions where there was well-defined electron density and hydrogen-bonding possibilities. Refinement and model quality statistics are listed in Table 3.

References

(1) Baba, M.; Tanaka, H.; De Clercq, E.; Pauwels, R.; Balzarini, J.; et al. Highly specific inhibition of human immunodeficiency virus type-1 by a novel 6-substituted acyclouridine derivative. *Biochem. Biophys. Res. Commun.* **1989**, *165*, 1375−1381.

(2) Miyasaka, T.; Tanaka, H.; Baba, M.; Hayakawa, H.; Walker, R. T.; et al. A novel lead for specific anti-HIV-1 agents: 1-[2-hydroxyethoxymethyl]-6-phenylthiothymine. *J. Med. Chem.* **1989**, *32*, 2507−2509.

(3) Pauwels, R.; Andries, K.; Desmytes, J.; Schols, D.; Kukla, M. J.; et al. Potent and selective inhibition of HIV-1 replication in vitro by a novel series of TIBO derivatives. *Nature* **1990**, *343*.

(4) Debyser, Z.; Pauwels, R.; Andries, K.; Desmytes, J.; Kukla, M.; et al. *Proc. Natl. Acad. Sci. U.S.A.* **1991**, *88*, 1451−1455.

(5) Balzarini, J. Current status of the non-nucleoside reverse transcriptase inhibitors of human immunodeficiency virus type 1. *Curr. Top. Med. Chem.* **2004**, *4*, 921−944.

(6) Ren, J. S.; Esnouf, R. M.; Garman, E.; Somers, D.; Ross, C.; et al. High-resolution structures of HIV-1 RT from four RT-inhibitor complexes. *Nat. Struct. Biol.* **1995**, *2*, 293−302.

(7) Esnouf, R.; Ren, J. S.; Ross, C.; Jones, Y.; Stammers, D.; et al. Mechanism of inhibition of HIV-1 reverse transcriptase by non-nucleoside inhibitors. *Nat. Struct. Biol.* **1995**, *2*, 303−308.

(8) Hopkins, A. L.; Ren, J.; Esnouf, R. M.; Willcox, B. E.; Jones, E. Y.; et al. Complexes of HIV-1 reverse transcriptase with Inhibitions of the HEPT series reveal conformational changes relevant to the design of potent non-nucleoside inhibitors. *J. Med. Chem.* **1996**, *39*, 1589−1600.

(9) Esnouf, R. M.; Ren, J.; Hopkins, A. L.; Ross, C. K.; Jones, E. Y.; et al. Unique features in the structure of the complex between HIV-1 reverse transcriptase and bis(heteroaryl)piperazine (BHAP) U-90152. *Proc. Natl. Acad. Sci. U.S.A.* **1997**, *94*, 3984−3989.

(10) Campiani, G.; Ramunno, A.; Maga, G.; Nacci, V.; Fattorusso, C.; et al. non-nucleoside HIV-1 reverse transcriptase (RT) inhibitors: past, present and future perspectives. *Curr. Pharm. Des.* **2002**, *8*, 615−657.

(11) De Clercq, E. Perspectives for non-nucleoside reverse transcriptase inhibitors (NNRTIs) in the therapy of HIV-1 infection. *Il Farmaco* **1999**, *54*, 26−45.

(12) De Clercq, E. The role of non-nucleoside reverse transcriptase inhibitors. (NNRTI) in the therapy of HIV-1 infections. *Antiviral Res.* **1998**, *38*, 153−179.

(13) Ho, D. D.; Neumann, A. U.; Perelson, A. S.; Chen, W.; Leonard, J. M.; et al. Rapid turnover of plasma virions and CD4 lymphocytes in HIV-1 infection. *Nature* **1995**, *373*, 123−126.

(14) Perelson, A. S.; Neumann, A. U.; Markowitz, M.; Leonard, J. M.; Ho, D. D. HIV-1 dynamics in vivo: virion clearance rate, infected cell life-span and viral generation time. *Science* **1996**, *271*, 1582−1586.

(15) Wei, X.; Ghosh, S. K.; Taylor, M. E.; Johnson, V. A.; Emini, E. A.; et al. Viral dynamics in human immunodeficiency virus type 1 infection. *Nature* **1995**, *373*, 117−112.

(16) Nájera, I.; Holguín, A.; Quiñones-Mateu, M. E.; Muñoz-Fernández, A.; Nájera, R.; et al. Pol gene quasispecies of human immunodeficiency virus: mutations associated with drug resistance in virus from patients undergoing no drug therapy. *J. Virol.* **1995**, *69*, 23−31.

(17) Johnson, V. A.; Brun-Vezinet, F.; Clotet, B.; Conway, B.; D'Aquila, R. T.; et al. Drug resistance mutations in HIV-1. *Top. HIV Med.* **2003**, *11*, 215−221.

(18) Bangsberg, D. R.; M. A.; Deeks, S. G. Paradoxes of adherence and drug resistance to HIV antiretroviral therapy. *J. Antimicrob. Chemother.* **2004**, *53*, 696−699.

(19) Domaoal, R. A.; Demeter, L. M. Structural and biochemical effects of human immunodeficiency virus mutants resistant to non-nucleoside reverse transcriptase inhibitors. *Int. J. Biochem. Cell Biol.* **2004**, *36*, 1735−1751.

(20) Schinazi, R. F.; Larder, B. A.; Mellors, J. W. Mutations in retroviral genes associated with drug resistance. *Int. Antiviral News* **1997**, *6*.

(21) Das, K.; Ding, J.; Hsiou, Y.; Clark, A. J.; Moereels, H.; et al. Crystal structures of 8-Cl and 9-Cl TIBO complexed with wild-type HIV-1 RT and 8-Cl TIBO complexed with the Tyr181Cys HIV-1 RT drug-resistant mutant. *J. Mol. Biol.* **1996**, *264*, 1085−1100.

(22) Hsiou, Y.; Das, K.; Ding, J.; Clark, A. J.; Kleim, J.; et al. Structures of Tyr188Leu mutant and wild-type HIV-1 reverse transcriptase complexed with the non-nucleoside inhibitor HBY 097: inhibitor flexibility is a useful design feature for reducing drug resistance. *J. Mol. Biol.* **1998**, *284*, 313−323.

(23) Ren, J.; Nichols, C.; Bird, L.; Chamberlain, P.; Weaver, K.; et al. Structural mechanisms of drug resistance for mutations at codons 181 and 188 in HIV-1 reverse transcriptase and the improved resilience of second generation non-nucleoside inhibitors. *J. Mol. Biol.* **2001**, *312*, 795−805.

(24) Spence, R. A.; Anderson, K. S.; Johnson, K. A. HIV-1 reverse transciptase resistance to non-nucleoside inhibitors. *Biochemistry* **1996**, *35*, 1054−1063.
(25) Maga, G.; Amecker, M.; Ruel, N.; Hübscher, U.; Spadari, S. Resistance to nevirapine of HIV-1 reverse transcriptase mutants: loss of stabilizing interactions and thermodynamics or steric barriers are induced by different single amino acid substitutions. *J. Mol. Biol.* **1997**, *274*, 738−747.
(26) Hsiou, Y.; Ding, J.; Das, K.; Clark, A. J.; Boyer, P.; et al. The Lys103Asn mutation of HIV-1 RT: a novel mechanism of drug resistance. *J. Mol. Biol.* **2001**, *309*, 437−445.
(27) Kleim, J.-P.; Bender, R.; Billhardt, U.-M.; Meichsner, C.; Riess, G.; et al. Activity of a novel quinoxaline derivative against human immunodeficiency virus type 1 reverse transcriptase and viral replication. *Antimicrob. Agents Chemother.* **1993**, *37*, 1659−1664.
(28) Kleim, J.-P.; Bender, R.; Kirsch, R. Preclinical evaluation of HBY 097, a novel non-nucleoside reverse transcriptase inhibitor of human immunodeficiency virus type 1 replication. *Antimicrob. Agents Chemother.* **1995**, *39*, 2253−2257.
(29) Jacobo-Molina, A.; Ding, J.; Nanni, R. G.; Clark, A. D., Jr.; Lu, X.; et al. Crystal structure of human immunodeficiency virus type 1 reverse transcriptase complexed with double-stranded DNA at 3.0 A resolution shows bent DNA. *Proc. Natl. Acad. Sci. U.S.A.* **1993**, *90*, 6320−6324.
(30) Yu, Q.; Ottmann, M.; Pechoux, C.; Le Grice, S.; Darlix, J.-L. Mutations in the primer grip of human immunodeficiency virus type 1 reverse transcriptase impair proviral DNA synthesis and virion maturation. *J. Virol.* **1998**, *72*, 7676−7680.
(31) Ghosh, M.; Jacques, P. S.; Rodgers, D. W.; Ottmann, M.; Darlix, J.-L.; et al. Alterations to the primer grip of p66 HIV-1 reverse transcriptase and their consequences for template-primer utilization. *Biochemistry* **1996**, *35*, 8553−8562.
(32) Jacques, P. S.; Wöhrl, B. M.; Ottmann, M.; Darlix, J.-L.; Le Grice, S. Mutating the "primer grip" of p66 HIV-1 reverse transcriptase implicates tryptophan-229 in the template-primer utilization. *J. Biol. Chem.* **1994**, *269*, 26472−26478.
(33) Powell, M. D.; Ghosh, M.; Jacques, P. S.; Howard, K. J.; Le Grice, S.; et al. Alanine-scanning mutations in the "primer grip" of p66 HIV-1 reverse transcriptase results in selective loss of RNA priming activity. *J. Biol. Chem.* **1997**, *272*, 13262−13269.
(34) Palaniappan, C.; Wisniewski, M.; Jacques, P. S.; Le Grice, S.; Fay, P. J.; et al. Mutations within the primer grip of HIV-1 reverse transcriptase results in a loss of RNaseH function. *J. Biol. Chem.* **1997**, *272*, 11157−11164.
(35) Pelemans, H.; Esnouf, R. M.; Parniak, M. A.; Vandamme, A.-M.; De Clercq, E.; et al. A proline-to-histidine substitution at position 225 of human immunodeficiency virus type 1 (HIV-1) reverse transcriptase (RT) sensitizes HIV-1 RT to BHAP U-90152. *J. Gen. Virol.* **1998**, *79*, 1347−1352.
(36) Fujiwara, T.; Sato, A.; el-Farrash, M.; Miki, S.; Abe, K.; et al. S-1153 inhibits replication of known drug-resistant strains of human immunodeficiency virus type 1. *Antimicrob. Agents Chemother.* **1998**, *46*, 1340−1345.
(37) Balzarini, J.; Pelemans, H.; Esnouf, R.; De Clercq, E. A novel mutation (F227L) arises in the reverse transcriptase of human immunodeficiency virus type 1 on dose-escalating treatment of HIV type 1-infected cell cultures with the nonnucleoside reverse transcriptase inhibitor thiocarboxanilide UC-781. *AIDS Res. Hum. Retroviruses* **1998**, *14*, 255−260.
(38) Pelemans, H.; Esnouf, R.; Dunkler, A.; Parniak, M. A.; Vandamme, A. M.; et al. Characteristics of the Pro225His mutation in human immunodeficiency virus type 1 (HIV-1) reverse transcriptase that appears under selective pressure of dose-escalating quinoxaline treatment of HIV-1. *J. Virol.* **1997**, *71*, 8195−8203.
(39) Kleim, J.-P.; Winkler, I.; Rosner, M.; Kirsch, R.; Rubsamen-Waigmann, H.; et al. In vitro selection for different mutational patterns in the HIV-1 reverse transcriptase using high and low selective pressure of the nonnucleoside reverse transcriptase inhibitor HBY 097. *Virology* **1997**, *231*, 112−118.
(40) Bacheler, L. T.; Anton, E. D.; Kudish, P.; Baker, D.; Bunville, J.; et al. Human immunodeficiency virus type 1 mutations selected in patients failing efavirenz combination therapy. *Antimicrob. Agents Chemother.* **2000**, *44*, 2475−2484.
(41) Ghosh, M.; Williams, J.; Powell, M. D.; Levin, J., G.; Le Grice, S. F. Mutating a conserved motif of the HIV-1 reverse transcriptase palm subdomain alters primer utilization. *Biochemistry* **1997**, *36*, 5758−5768.
(42) Wöhrl, B. M.; Krebs, R.; Thrall, S. H.; Le Grice, S. F.; Scheidig, A. J.; et al. Kinetic analysis of four HIV-1 reverse transcriptase enzymes mutated in the primer grip region of p66. Implications for DNA synthesis and dimerization. *J. Biol. Chem.* **1997**, *272*, 17581−17587.
(43) Hopkins, A. L.; Ren, J.; Tanaka, H.; Baba, M.; Okamato, M.; et al. Design of MKC-442 (emivirine) analogues with improved activity against drug-resistant HIV mutants. *J. Med. Chem.* **1999**, *42*, 4500−4505.
(44) Pelemans, H.; Esnouf, R.; De Clercq, E.; Balzarini, J. Mutational analysis of trp-229 of human immunodeficiency virus type 1 reverse transcriptase (RT) identifies this amino acid residue as a prime target for the rational design of new non-nucleoside RT inhibitors. *Mol. Pharmacol.* **2000**, *57*, 954−960.
(45) Harrigan, P.; Salim, M.; Stammers, D.; Wynhoven, B.; Brumme, Z.; et al. A mutation in the 3′ region of the human immunodeficiency virus type 1 reverse transcriptase (Y318F) associated with nonnucleoside reverse transcriptase inhibitor resistance. *J. Virol.* **2002**, *76*, 6836−6840.
(46) Pelemans, H.; Esnouf, R. M.; Jonckheere, H.; De Clercq, E.; Balzarini, J. Mutational analysis of Tyr-318 within the non-nucleoside reverse transcriptase inhibitor binding pocket of human immunodeficiency virus type I reverse transcriptase. *J. Biol. Chem.* **1998**, *273*, 34234−34239.
(47) Ren, J.; Esnouf, R.; Hopkins, A.; Ross, C.; Jones, Y.; et al. The structure of HIV-1 reverse transcriptase complexed with 9-chloro-TIBO: lessons for inhibitor design. *Structure* **1995**, *3*, 915−926.
(48) Tanaka, H.; Walker, R. T.; Hopkins, A. L.; Ren, J.; Jones, E. Y.; et al. Allosteric inhibitors against HIV-1 reverse transcriptase: design and synthesis of MKC-442 analogues having an omega-functionalized acyclic structure. *Antivir. Chem. Chemother.* **1998**, *9*, 352−332.
(49) Ren, J.; Nichols, C.; Bird, L. E.; Fujiwara, T.; Sugimoto, H.; et al. Binding of the second generation non-nucleoside inhibitor S-1153 to HIV-1 reverse transcriptase involves extensive main chain hydrogen bonding. *J. Biol. Chem.* **2000**, *275*, 14316−14320.
(50) Osbourne, A. G.; Buley, J. M.; Clarke, H.; Dakin, R. C. H.; Price, P. I. 2,4-dihalogenoquinolines. Synthesis, orientation effects and ^{1}H and ^{13}C NMR spectral studies. *J. Chem. Soc., Perkins Trans. 1* **1993**, *22*, 2747−2755.
(51) Hunter, C. A.; Sander, J. K. M. The nature of $\pi-\pi$ interactions. *J. Am. Chem. Soc.* **1990**, *112*, 5525−5534.
(52) Freeman, G. A.; Andrews, C. A., III; Hopkins, A. L.; Lowell, G. S.; Gonzales, S. S.; et al. Design of non-nucleoside inhibitors of HIV-1 reverse transcriptase with improved drug resistance properties. 2. **2003**, in press.
(53) Goodford, P. J. A computational procedure for determining energetically favourable binding sites on biologically important macromolecules. *J. Med. Chem.* **1985**, *28*, 829−857.
(54) Powell, M. J. D. Restart procedures for the conjugate gradient method. *Math. Program.* **1977**, *12*, 241−254.
(55) Brünger, A. T. *X-PLOR*; Yale University: New Haven.
(56) Daresbury Laboratory, D., Warrington, U.K. Chemical Database Service, CLRC.
(57) Tramontano, E.; Cheng, Y.-C. HIV-1 reverse transcriptase inhibition by a dipyridodiazepinone derivative: BI−RG-587. *Biochem. Pharmacol.* **1992**, *43*, 1371−1376.
(58) Spira, T. J.; Bozeman, L. H.; Holman, R. C.; Warfield, D. T.; Phillips, S. K.; et al. Micromethod for assaying reverse transcriptase of human T-cell lymphotropic virus type III/lymphadenopathy-associated virus. *J. Clin. Microbiol.* **1987**, *25*, 97−99.
(59) Averett, D. R. Anti-HIV compounds assessment by two high capacity assays. *J. Virol. Methods* **1989**, *23*, 263−276.
(60) Schwartz, O. A rapid and simple colorimetric test for the study of anti-HIV agents. *AIDS Res. Hum. Retroviruses* **1988**, *4*, 441−447.
(61) Daluge, S. M.; Purifoy, D. J. M.; Savina, P. M.; St. Clair, M. H.; Parry, N. P.; et al. 5-Chloro2′3′-dideoxy-3′-fluorouridine 935U83, a selective anti-human immunodeficiency virus agent with an improved metabolic and toxicological profile. *Antimicrob. Agents Chemother.* **1994**, *38*, 1590−1603.
(62) Dornsife, R. E. Anti-human immunodeficiency virus synergism by zidovudine (3′-azidothymidine) and didanosine (dideoxyinosine) contrasts with the additive inhibition of normal human marrow progenitor cells. *Antimicrob. Agents Chemother.* **1991**, *35*, 322−328.
(63) Stammers, D. K.; Somers, D. O. N.; Ross, C. K.; Kirby, I.; Ray, P. H.; et al. Crystals of HIV-1 reverse transciptase diffracting to 2.2 Å resolution. *J. Mol. Biol.* **1994**, *242*, 586−588.
(64) Otwinowski, Z. Oscillation data reduction program. *Data Collection and Processing*; SERC Daresbury Laboratory: Warrington, England, 1993; pp 56−62.
(65) Brunger, A.; Adams, P.; Clore, G.; DeLano, W.; Gros, P.; et al. Crystallography & NMR system: A new software suite for macromolecular structure determination. *Acta Crystallogr. D Biol. Crystallogr.* **1998**, *54*, 905−921.
(66) Engh, R. A.; Huber, R. Accurate bond and angle parameters for X-ray protein structure refinement. *Acta Crystallogr.* **1991**, *A47*, 392−400.
(67) Jones, T. A. Interactive computer graphics: FRODO. *Methods Enzymol.* **1985**, *115*, 157−171.

JM040071Z